Comparative 3D ultrastructure of *Plasmodium falciparum* gametocytes

Felix Evers[1], Rona Roverts[2,3], Cas Boshoven[1], Mariska Kea-te Lindert[2,3], Julie M.J. Verhoef[1], Robert E. Sinden[4], Anat Akiva[2,3], Taco W.A. Kooij[1*]

[1]Department of Medical Microbiology, Radboudumc Center for Infectious Diseases, Radboud University Medical Center, Nijmegen, The Netherlands.
[2]Electron Microscopy Center, RTC Microscopy, Radboud University Medical Center, Nijmegen, the Netherlands.
[3]Department of Medical Biosciences, Radboud University Medical Center, Nijmegen, the Netherlands.
[4]Department of Life Sciences, Imperial College London, London, UK.

* taco.kooij@radboudumc.nl

Abstract

Despite the enormous significance of malaria parasites for global health, some basic features of their ultrastructure remain obscure. In this study, we apply high-resolution volumetric electron microscopy to examine and compare the ultrastructure of *Plasmodium falciparum* gametocytes of both genders and in different stages of development as well as the more intensively studied asexual blood stages revisiting previously described phenomena in 3D. In doing so, we challenge the widely accepted notion of a single mitochondrion by demonstrating the presence of multiple mitochondria in gametocytes. We also provide evidence for a gametocyte-specific cytostome variant. Furthermore, we generate, among other organelles, the first 3D reconstructions of endoplasmic reticulum (ER), Golgi apparatus, and extraparasitic structures in gametocytes. Assessing interconnectivity between organelles, we find frequent structural appositions between the nucleus, mitochondria, and apicoplast. We provide evidence that the ER is a promiscuous interactor with numerous organelles and the trilaminar membrane of the gametocyte. Public availability of these volumetric electron microscopy resources of wild-type asexual and sexual blood-stage malaria parasites will facilitate reinterrogation of this global dataset with different research questions and expertise. Taken together, we reconstruct the 3D ultrastructure of *P. falciparum* gametocytes in high detail and shed light on the unique organellar biology of these deadly parasites.

Introduction

Parasites from the genus *Plasmodium* are the causative agents of malaria. This mosquito-borne infectious disease remains a huge burden on global public health with more than 200 million cases and >600 thousand fatalities in 2021 alone[1, 2]. Humanity's efforts to combat this disease have shown impressive results during the years 2000 – 2015 but have since stalled. This is largely driven by continuing emergence of resistance to all frontline antimalarials[3] as well as the inability of most antimalarials to combat directly the asymptomatic but transmissible sexual stages[4]. To stop parasite transmission and eliminate malaria, there is an urgent need for drugs with novel mechanisms of action, particularly those that are effective against sexual stages. The apicomplexan phylum, among which are the malaria parasites, diverged very early in eukaryotic evolution and some basic cellular processes and structures are comparatively poorly understood despite their immense significance for global health. In particular, *Plasmodium* organelle biology has been shown to deviate from standard eukaryotic models and varies drastically between the different life-cycle stages. Furthermore, Apicomplexa are almost exclusively parasitic, which drives additional divergence in cellular features related to their survival strategy, such as feeding, locomotion, secretion, invasion, and adaptation to their respective hosts. As a result, we are in the situation where there is urgency to find drug or vaccine candidates for cellular systems that are relatively poorly understood. In the case of *Plasmodium*, this holds particularly true for life-cycle stages, like the sexual gametocyte stages, that are less accessible than the pathogenic asexual blood-stage parasites (ABS).

Classical electron microscopy studies in the period from 1965-2000 provided key insights into the ultrastructure of malaria parasites and laid the groundwork for much of our understanding of sexual-stage biology[5-8]. There have been a few noteworthy serial sectioning electron microscopy (ssEM) applications[9-12], however, these early studies lacked the advanced quantitative, volumetric, and computational methods available today and did not have the context of our current molecular understanding of malaria parasite biology. With the advent of novel and, more importantly, increasingly accessible high-resolution volumetric approaches such as focused ion beam milling - scanning electron microscopy (FIB-SEM), serial block-face scanning electron microscopy (SBF-SEM), array tomography (AT), and expansion microscopy (ExM), we have made great advances in recent years. Features of ABS and oocysts and their respective replication strategies have been investigated via FIB-SEM with great success[13, 14]. ssEM and AT have recently been applied to elucidate the reputed role of nuclear microtubules in driving the characteristic elongation of developing gametocytes[15] and general measurements of gametocytes and insights underpinning the inner membrane complex (IMC) have been gained using SBF-SEM[16]. ExM has been used to elucidate microtubule dynamics across gametocyte development and during activation, and immunofluorescence-based studies have demonstrated that the mitochondrion dramatically branches and enlarges in the gametocyte stages[17-19]. Additionally, electron micrographs have shown that in contrast to the acristate mitochondrion in ABS, the gametocyte mitochondrion is highly cristate[6, 20, 21]. Yet, other organelles, such as the endoplasmic reticulum (ER), the Golgi apparatus (Golgi), and the cytostome, and their interconnectivity have not been subject to specific microscopic investigations in gametocytes and our general understanding of their morphology and putative interactions is largely derived from model eukaryotes or extrapolated from *Plasmodium* ABS.

In this study, we investigate the ultrastructure of gametocytes using high resolution FIB-SEM and ssSEM volumetric imaging. We compare our ultrastructural gametocyte findings with our ABS data and other

high-resolution volumetric studies. In doing so, we find evidence for a morphologically distinct cytostome in gametocytes, multiple mitochondria per cell, indications for widespread inter-organelle interactions, generate high-resolution renderings of various organelles and visualize 3D morphology and distribution of external structures in gametocytes. Additionally, we aim to create a reusable image resource for the malaria research community to investigate more cells from the FIB-SEM and ss-SEM data, contrast their own findings with a reference point, and reinterrogate the datasets with their specific biological question, perspective, and expertise.

Results and Discussion

General morphology of the gametocyte

The mature gametocytes show their typical crescent shape that is well known from light microscopy-based imaging (Fig. 1A-B, Movies S1-2). The surrounding red blood cell (RBC) also conformed to this general shape, with the Laveran's bib, a narrow ridge spanning between the tips of the parasite crescent, being evident in all stage IV and V gametocytes (Fig. 2). We also identified contorted mature gametocytes with a twisted appearance including a narrowing of the cytoplasm, a frequent aberrant morphology known from Giemsa preparations of gametocyte cultures (Fig. S1). We were surprised to find that aside from the deviating morphology, no other signs of poor health or differences of internal structures could be recognized in these contorted gametocytes. Immature gametocyte stages (stage II-IV) were identified based on their well-characterized straighter or more compact appearance and incomplete inner membrane complex (Fig. S2). With increased maturity, the overall electron density of the RBC cytoplasm decreases and an electron lucent corona surrounding the gametocyte becomes apparent, indicative of hemoglobin depletion (Fig. S3). While we were unable to confidently assign sexes to earlier stages, we relied on differing patterns of hemozoin distribution together with the frequency and appearance of osmiophilic bodies (OBs) to differentiate male and female stage IV/V gametocytes. Whereas previously cytoplasmic density of ribosomes[22] was widely used to discriminate genders, we could not detect such differences in our preparations. OBs are vesicles that are abundant in females and thought to play a role during gametocyte egress from the RBC. *P. falciparum* males have been suggested to contain fewer OBs or even lack them completely[5, 23]. Our data show that *P. falciparum* males, contain vesicles that share morphological characteristics with OBs (Fig. 1B, Fig. S4A, Movie S2). As in *Plasmodium berghei*, these structures are much fewer in number in males than in females[24]. Furthermore, all or almost all OBs in male gametocytes have a "tail" that occasionally interconnects the vesicles - which is found only in a small subset of OBs in females (Fig. S4). This tail has been observed previously in a thin section of a female *Plasmodium cathemerium* gametocyte and a *Plasmodium gallinaceum* gametocyte[25] but is largely absent from previous microscopic data of *P. falciparum* gametocytes. It would be interesting to investigate further whether these different observations reflect differences in underlying biology of the analyzed parasites or methodological differences. One possible explanation is that paucity of prior observations might stem from a higher likelihood of identification in high-resolution volumetric data as opposed to individual thin slices or differing staining procedures that make these structures visible. In the rodent malaria parasite, *P. berghei,* male osmiophilic bodies have been shown to have a distinct but overlapping proteome compared to OBs identified in female gametocytes[24]. However, no morphological differences were evident from the presented representative micrographs. We hypothesize that the putative OBs identified in male *P. falciparum* gametocytes also differ in protein composition as males do not stain positive for the Pfg377 protein that readily stains OBs of female gametocytes[23]. Supporting this hypothesis a recent preprint suggests presence of two

122 functionally distinct subtypes of vesicles with different proteomes that aid in gametocyte egress, one of
123 which – in line with our data - does not show any evidence for gender specificity[26].

124 To compare our gametocyte reconstructions with the more extensively studied ABS[13], we reconstructed
125 two representative cells: a schizont that is still undergoing nuclear division and a fully segmented
126 schizont, (Fig. 1C-D, Movie S3). Overall 3D morphology and appearance of the structures in individual
127 slices match those observed by Rudlaff *et al.*[13] (publicly available from EMPIAR-10392). The schizont
128 contains ten distinct nuclei and extensive mitochondrial and apicoplast networks that permeate the
129 whole cell. The segmenter is comprised of 31 fully formed daughter merozoites, each containing
130 mitochondrion, apicoplast, rhoptry pair, ER, micronemes, and nucleus, and an additional (32nd)
131 merozoite that lacks a nucleus. Even at this late stage of development, without exception, each
132 merozoite is still connected to the residual body that surrounds the food vacuole (Fig. 1C, Movie S3).
133 This connectivity is highlighted by one merozoite that is connected to the residual body through an
134 elongated neck/tube (Fig. S5A). Furthermore, the residual body is connected to the RBC cytoplasm via
135 two continuous tubes, presumably facilitating continued sustenance to the daughter merozoites until
136 rupture. Our data also contain occasional extracellular merozoites, most likely due to schizonts rupturing
137 in the interval between magnetic separation and fixation. Comparing released extracellular to the
138 intraerythrocytic merozoites, we find that volumes of the overall merozoite and individual organelles
139 are very similar, supporting the notion that the corresponding segmented schizont is close to full
140 maturity (Fig. 1D). The only dimension on which the extracellular and intracellular merozoites differ is
141 that the extracellular merozoite is spherical while the average intracellular merozoite conforms to a
142 tooth-like shape, likely due to space constraints in the schizont and to maintain a connection to the
143 residual body throughout development. This observation is consistent with data from *Plasmodium*
144 *knowlesi* and a post PVM-rupture *P. falciparum* schizont[13, 27]. Other characteristics of the ABS are
145 described in comparison with the gametocyte in other sections below.

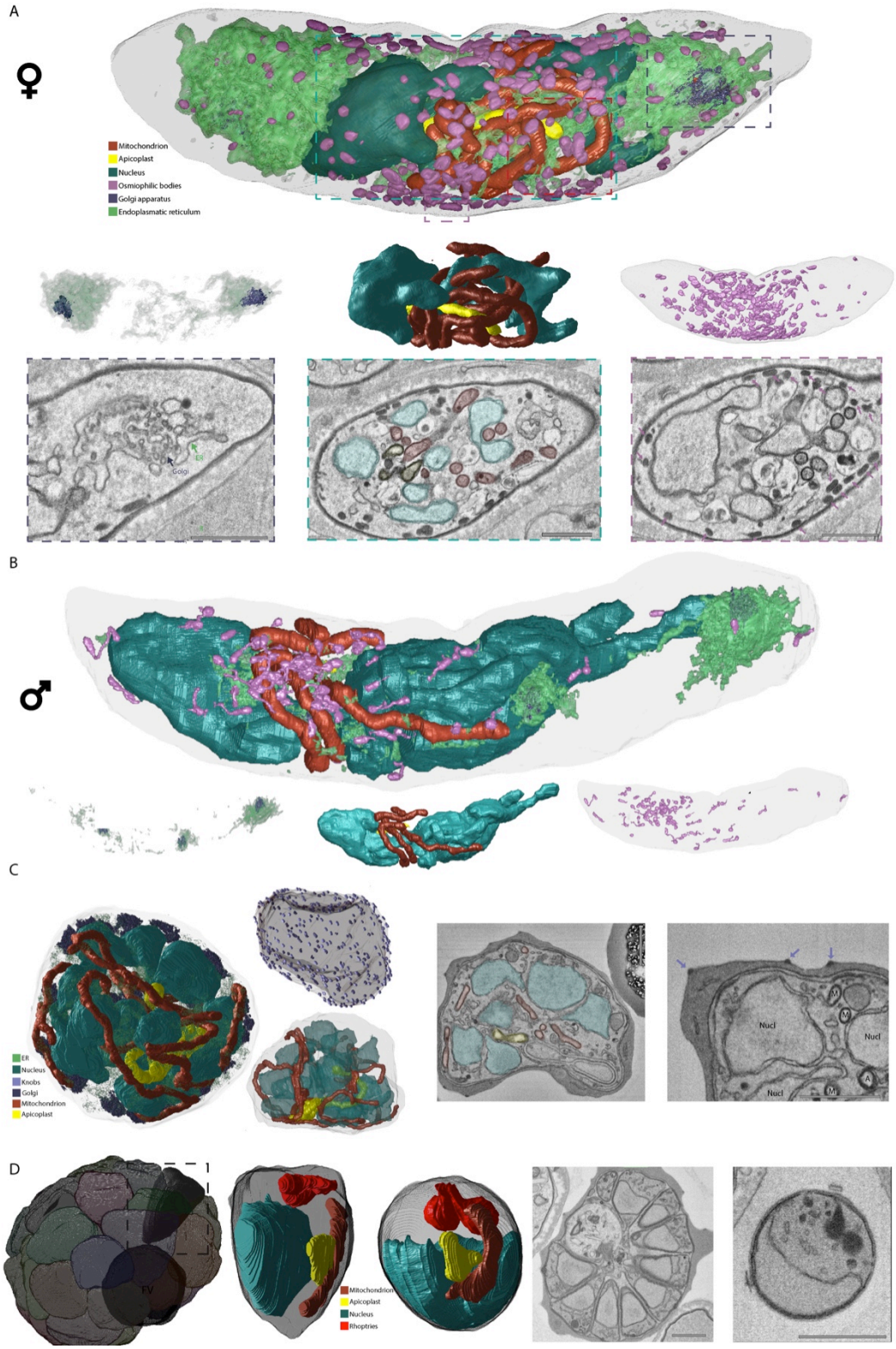

Figure 1 | **Ultrastructural features and renderings of mature gametocytes, schizont and segmented schizont.**
A. Rendering of ultrastructural features of a mature female gametocyte and specific renderings of Golgi and ER distribution (left panel), relation of nucleus/apicoplast/mitochondrion (middle panel) as well as distribution and appearance of osmiophilic bodies. Appearance of rendered structures in exemplary micrographs is matched to rendered features through color-coded

151 dashed lines. Scale bars = 1 µm. **B.** Rendering of ultrastructural features of a mature male gametocyte and specific renderings as
152 in (A). Note the relative paucity of ER, Golgi, and osmiophilic bodies relative to the female gametocyte. The osmiophilic bodies
153 differ morphologically with overall thinner appearance and frequent tail-like extensions. **C.** Rendering of ultrastructural features
154 of an early schizont and specific rendering of relation of nucleus/apicoplast/mitochondrion as well as individual knob
155 distribution. Appearance of ultrastructural features is shown in two exemplary micrographs. Scale bars = 1 µm.
156 M = Mitochondrion; ER = Endoplasmic reticulum; Nucl = Nucleus; FV = Food vacuole. **D.** Rendering of daughter merozoites
157 within a segmented schizont and rendering of one intracellular and one extracellular merozoite with ultrastructural features.
158 Overview on appearance of the two merozoite shapes is shown in two exemplary micrographs. Scale bars = 1 µm.

159 **Parasite-induced modifications of the red blood cell**

160 RBCs infected with mature gametocytes contain flat, membranous disks (Fig. 2A-B) that differ from the
161 characteristic membranous stacks called Maurer's clefts we observed in ABS-infected RBCs (Fig. 2C). In
162 gametocytes of both genders, extraparasitic structures were less frequent, generally larger but
163 heterogenous in size and unevenly distributed within the RBC cytoplasm (Fig. 2A-B). We consistently find
164 a higher density of extraparasitic structures in the Laveran's bib that spans between the two ends of the
165 mature gametocyte[28]. This matches results of previous work that found accumulation of a class of
166 exported proteins to this subcellular location[29]. Furthermore, we find an occurrence of a 'Garnham
167 body', a rare gametocyte exclusive structure originally discovered in 1933 with still unknown functional
168 significance[30] (Fig. S6). Our data confirm the highly membranous appearance of the Garnham body
169 described in previous micrographs and specifically we identify four double membranes. However, we
170 found no associated hemozoin, which was identified in some light microscopy examples[5, 6, 22, 31] (Fig. S6A-
171 B). The Garnham body was found adjacent to but not within the Laveran's bib, at a site devoid of IMC
172 and situated in the vicinity of the opening of the cytostome (Fig. S6C). The presence of a Garnham body
173 in the RBC also coincides with electron dense protrusions of the parasite vacuolar membrane radiating
174 in all direction from the parasite and a membranous electron lucent compartment within the parasite,
175 that were observed in no other cells (Fig. S6A-B). These concurrent exclusive features could indicate
176 Garnham bodies to be a sign of an unhealthy gametocyte and/or RBC or suggestive of a rare subtype in
177 gametocyte populations.

178 Consistent with published literature, the plasma membrane of gametocyte-infected RBCs is not visibly
179 modified, while the ABS-infected cells are thoroughly covered by uniformly distributed knobs, which are
180 proteinaceous parasite-derived protrusions that mediate cytoadherence of ABS-infected RBCs[32] (Fig. 1C,
181 Movie S3). Reconstructions suggest a total of 390 knobs on the surface of the schizont-infected RBC
182 corresponding to 2.9 knobs/μm^2, which is in line with previous measurements obtained for NF54-
183 infected RBCs via atomic force microscopy[33]. The overall surface profile of the segmenter-infected RBC
184 appeared more uneven with more peaks and valleys compared to the developing schizont, while
185 gametocyte-infected RBCs appeared to have a smoother surface profile than either (Fig. S5B-D). As
186 anticipated, the trilaminar membrane architecture of the gametocyte-RBC interface, consisting of the
187 parasite vacuolar membrane (PVM), the parasite plasma membrane (PM) and the IMC, is evident from
188 the micrographs. Localized areas of further thickened IMC membrane might represent the leading edge
189 of IMC plates[16] while areas without IMC cover in immature stages suggest ongoing IMC plate biogenesis
190 (Fig. S7A-B). In mature stages, we occasionally find similar IMC overhangs of unknown significance
191 (Fig. S7C).

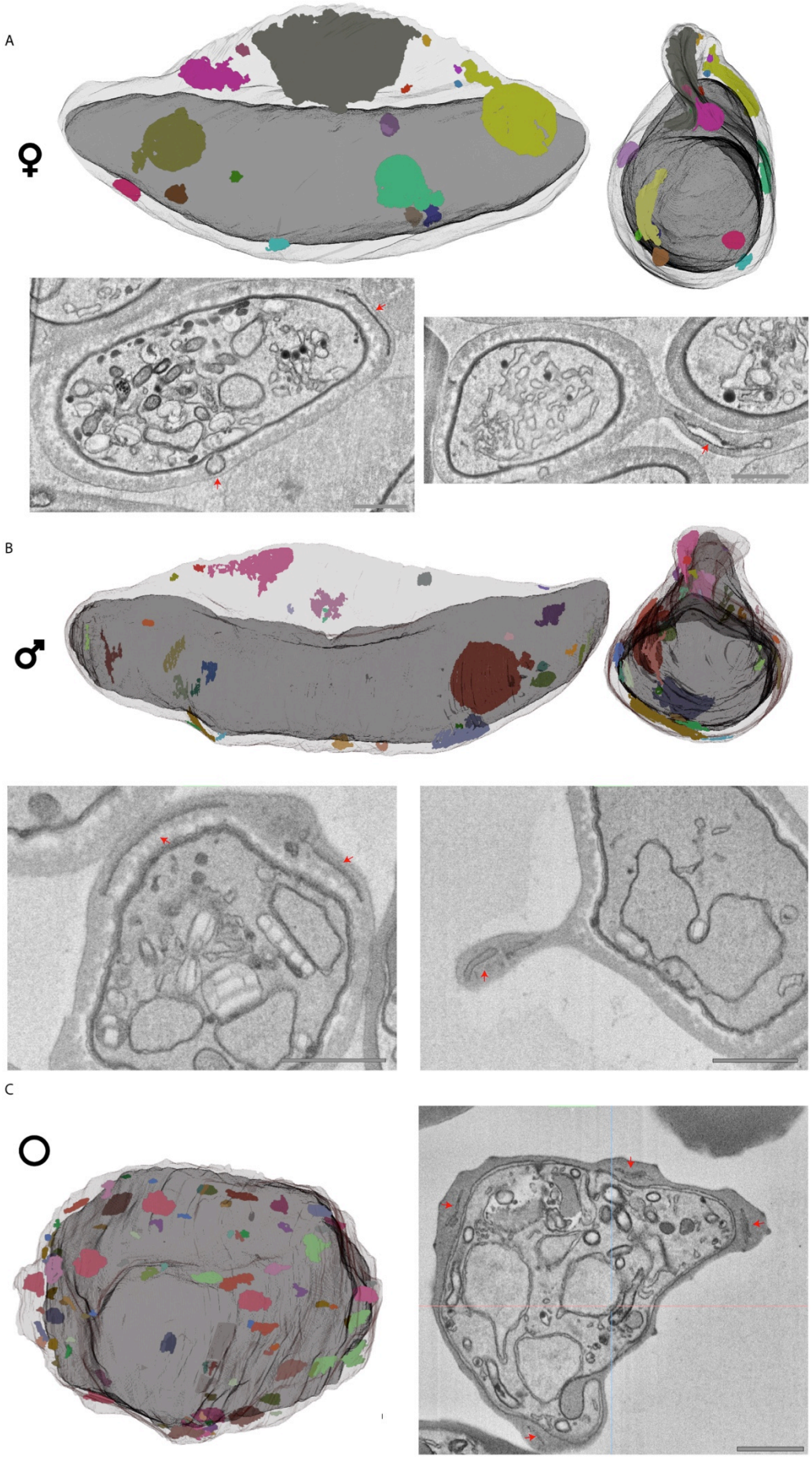
A
♀
B
♂
C
○

193 *Figure 2* | **Extraparasitic structures differ in gametocytes and ABS.**
194 (**A**) Mature female and (**B**) male gametocyte, and (**C**) schizont rendered with RBC outline and extraparasitic structures in
195 different color for each membrane structure. Gametocyte renderings are shown from two angles. Examples of extraparasitic
196 structures in micrographs are highlighted with red arrows. Scale bars = 1 µm.

197 **The gametocyte cytostome**

198 RBC-parasite interactions are not restricted to host-cell modification, but also include the internalization
199 and digestion of host-cell cytoplasm to fuel parasite growth. An unusual feeder organelle, the cytostome
200 (meaning cell mouth), facilitates this uptake of RBC cytoplasm in ABS[12]. In our micrographs of ABS and
201 other studies[34], the cytostome presents itself as a hemoglobin filled tube surrounded by a double-
202 membrane and possessing an electron dense "neck", called the cytostomal collar, at the invagination
203 site (Fig. S8). Gametocytes similarly rely on hemoglobin internalization and digestion. Putative
204 morphologically diverse cytostomes have been assigned in past EM studies[5, 6]. When trying to assign the
205 cytostome in mature gametocytes, we came across likely yet distinct candidate structures. Presenting a
206 clear invagination of the parasite membranes, the structures are always surrounded by extensive ER but
207 otherwise can be subdivided into three categories (Fig. 3A). In 44% of the evaluated examples (n = 50),
208 the organelle has a membrane delimited electron dense ring that is 100-160nm thick and connected to
209 the RBC cytoplasm while the lumen circumscribed by the ring appears electron lucent and can
210 occasionally contain further membranous or dark stained structures. In 40% of the cases the structures
211 had a more ABS-like appearance with no clear delineation into ring and lumen but circular grooves on
212 the inside of the membrane that are absent in the ABS cytostome potentially indicative of future
213 emergence of the ring structure. In the remainder the ring is relatively larger with inconsistent thickness
214 and a smaller electron lucent internal lumen potentially representing an in-between state. Furthermore,
215 it appears that each gametocyte that we have fully imaged only contains a single cytostome of any of
216 these three gametocyte-specific subtypes. Conversely, in ABS multiple cytostomes have been reported[35]
217 and are also evident from our data with a maximum of seven cytostomes per cell (Fig. S8, panel 3).
218 Interestingly, in one example of a developing gametocyte, we find both a canonical ABS-type cytostome
219 and a gametocyte variant (Fig. 3B). This observation suggests that the structure we identified in
220 gametocytes might be entirely distinct from the cytostome. In mature stages, hemoglobin
221 internalization is largely finished and consequently the cytostome may no longer be required for its
222 canonical purpose. It is tempting to speculate that this cytostome variant is instead involved in host lipid
223 acquisition, as parasite lipid content dramatically increases throughout gametocytogenesis[36]. This would
224 also offer a plausible explanation for the ER, as the primary site of lipid metabolism, consistently
225 surrounding the cytostome and would suggest that the occasional dark contents of the lumen seen in
226 our preparations are (osmiophilic) lipids.

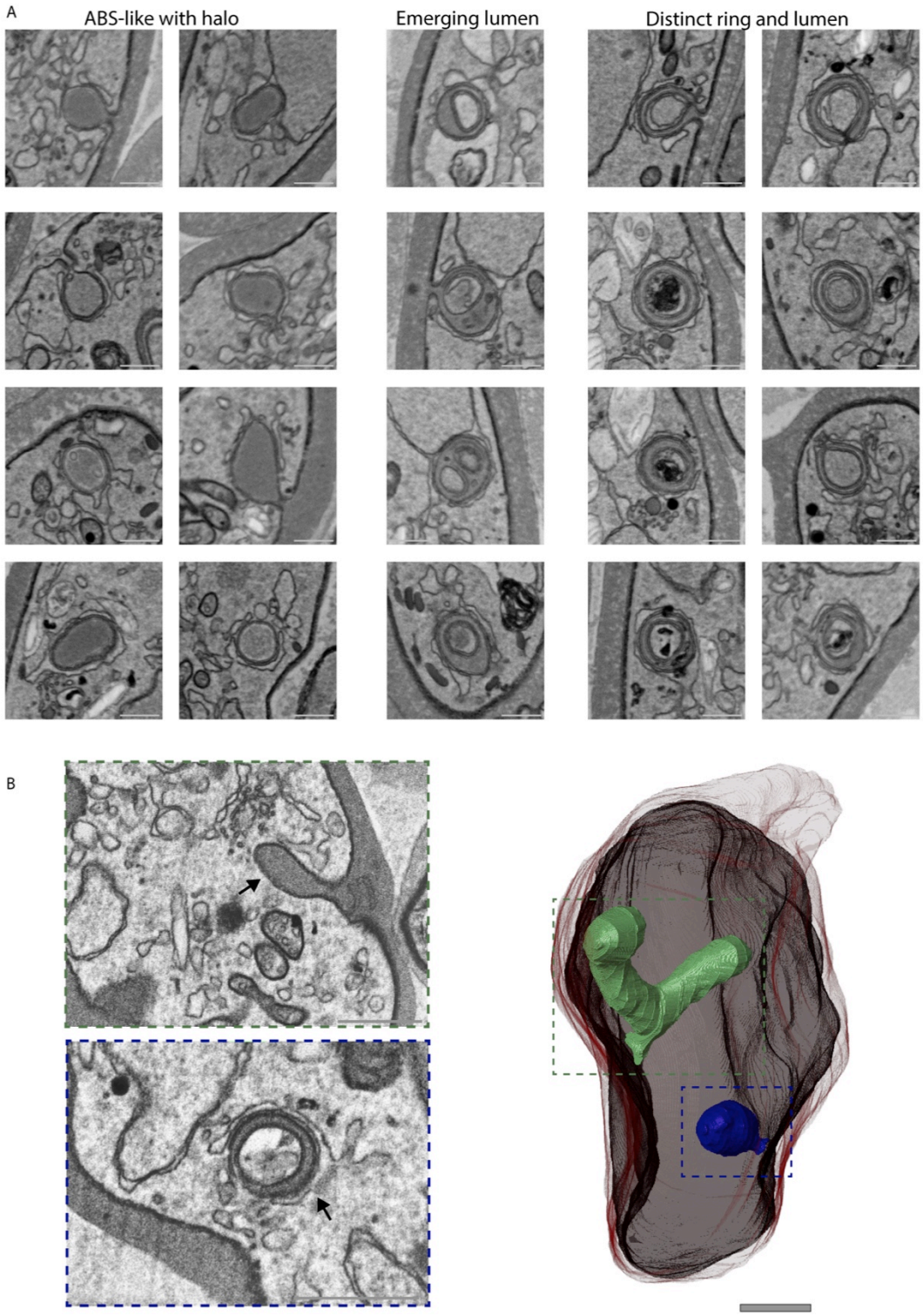

Figure 3 | **The gametocyte cytostome.**
A. Exemplary micrographs of the cytostome in 20 different gametocytes subdivided into three categories. **Left**: Cytostome without further membrane delineation in lumen, relatively homogenous lumen and circular grooves that could indicate future emergence of ring. **Middle**: Relatively large membrane electron dense ring and small electron lucent lumen. Ring is continuous with RBC cytosol, putative intermediate state. **Right**: Electron dense ring with homogenous thickness and lumen with heterogenous content. Ring is continuous with RBC cytosol. All categories have close association of ER unlike the ABS cytostome. Scale bars = 0.1 µm. **B.** Rendering of a developing gametocyte that contains both a canonical ABS cytostome and a

235 cytostome with distinct ring and lumen. The ABS cytostome (green) is characterized by homogenous dark lumen and
236 continuation of the parasite membrane that forms the invagination. The gametocyte cytostome (blue) is characterized by a
237 bulbous shape and distinct electron dense ring with electron lucent lumen.

238 **The gametocyte ER and Golgi-apparatus**

239 Universally the ER is an extensive interconnected organelle continuous with the nuclear envelope that
240 serves as a transport hub, hosts various critical cellular functions, is widely connected with other
241 organelles, and even acts as a mediator of organellar interactions[37]. We find that the ER in both
242 developing gametocytes and mature female gametocytes is extensive and occupies large parts of the
243 cell, similar to the schizont (Fig. 1A, Fig. S2, Movie S1). The mature male gametocyte on the other hand
244 appears to contain much less ER, which is in line with previous observations and proteomic data[38, 39]
245 (Fig. 1B, Movie S2). It is noteworthy that in the mature female gametocyte, the ER is most dense in the
246 polar regions of the parasite. This coincides with the distribution of a closely associated organelle, the
247 Golgi, which, in *Plasmodium*, takes the rudimentary form of dispersed unstacked cisternae and is
248 recognizable as a smooth membraned vesicle cluster[22, 40-42]. In females, the Golgi is predominantly found
249 in two distinct clusters at both polar ends, while in the mature male it appears distributed across smaller
250 clusters, similar to the developing gametocytes that also have a more widespread distribution.
251 Compared to the gametocytes, the Golgi is much more extensive in the schizont and found in evenly
252 dispersed clusters around the cell (Fig. 1C, Movie S3).

253 **The ER as a putative path across the IMC**

254 The ER also facilitates the extensive host-cell remodeling that occurs in ABS. In *P. falciparum*, an
255 estimated lower bound of 300 unique proteins, >5% of the proteome, is exported to the host cell to
256 modify aspects such as cytoadhesion, the host cytoskeleton, or nutrient permeability[43]. Proteins
257 destined for export are processed in the ER and delivered to the PM via vesicular transport and then
258 forwarded to the *Plasmodium* Translocon of EXported proteins (PTEX) in the PVM, which translocates
259 the proteins into the host cell. While extensively researched in ABS, we know relatively little about how
260 this process translates to the gametocyte situation. Maurer's clefts appear absent in gametocytes,
261 possibly replaced by other cleft-like structures[44], and the gametocyte exportome is distinct from the ABS
262 exportome[45]. Whilst protein export machinery is essential for early gametocyte development[46, 47],
263 protein export has not been conclusively demonstrated in gametocytes beyond stage III. Indeed, as the
264 IMC cover increases, staining of the export machinery on the PVM becomes less pronounced or even
265 disappears completely in *P. falciparum* and *P. berghei* gametocytes, respectively[45, 48]. If protein export
266 still happens in late gametocyte stages the mechanism by which the additional barrier presented by the
267 IMC is overcome, is currently unknown[49]. In mature gametocytes, we frequently find sites at which the
268 ER runs very close to or is in direct contact with the parasite membrane (Fig. S9). From our observations
269 this interaction can manifest in a few different forms. The most frequent observation is that ER directly
270 contacts the IMC, leading to a continuum between these two compartments as well as local disruption
271 of the IMC (Fig. S9A). Less frequently but consistently, we observe "budding" of a piece of ER that
272 contacts the parasite membrane (Fig. S9B). These local continuities between ER and IMC might
273 represent a mechanism to bridge the IMC and allow canonical ER-derived vesicle fusion with the PM or
274 facilitate alternative means of protein export. In developing gametocytes with incomplete IMC cover, we
275 find that all extension sites are subject of extensive ER interaction with the nascent IMC (Fig. S9D) This is
276 in line with previous EM-based observations that the outer nuclear envelope interacts with nascent IMC
277 and the PPM in developing gametocytes[15] and with immunofluorescence microscopy data suggesting

278 regions of ER contact with the IMC[50]. Even in mature gametocytes with complete IMC cover we too find
279 sites at which ER converts to electron dense material that resembles IMC (Fig. S9C). Taken together,
280 these observations, while anecdotal, provide further evidence for a dynamic interplay between ER and
281 IMC biogenesis or maintenance and suggest a speculative mechanism to bridge the additional
282 membrane layer in gametocytes for protein export.

283 **Features of *Plasmodium* mitochondria**

284 In gametocytes, the mitochondria are readily recognizable based on their cristate appearance and two-
285 layered membrane. The cristae appear to have some degree of interconnectivity, consistent with
286 previous interpretations of tubular cristae, but the small size of the structures and variability between
287 slices, even at a z-resolution of 15 nm, makes clear assertions of connectivity challenging (Fig. S10B,
288 Movies S4-5). While edges of the individual cristae are more evident from the lower noise serial
289 sectioning data, the low z-resolution does not allow for reconstruction of their morphology (Fig. S10A).
290 In the individual micrographs, the cristae are similar to the recently described bulbous cristae in the
291 related apicomplexan parasite *Toxoplasma gondii*[51]. In line with previous reports, the mitochondrion is
292 double-membraned yet acristate in ABS. In both ABS and gametocyte mitochondria, we regularly
293 identify electron dense mitochondrial granules (EDMGs) that appear in clusters of 1-10 EDMGs and are
294 heterogeneous in volume with a notably smaller size, propensity to be more separate and more slender
295 in shape in ABS (Fig. 4A) [52, 53]. While they have not been described before, they are readily recognizable
296 in the image stacks of schizonts made public by Rudlaff *et al.*[13], indicating it is not a unique feature of
297 our preparations. The electron dense appearance could suggest that these granules are sub-
298 compartments that are either very proteinaceous or contain polysaccharides, lipids, or mitochondrially
299 relevant metals such zinc, calcium, copper, and/or iron. *P. falciparum* mitochondria have been shown to
300 play a role in calcium mobilization and storage[54] and so-called matrix granules that are heavily enriched
301 in calcium phosphate have been found in mammalian mitochondria[55]. In parasites isolated from fish
302 digestive tracts, similar mitochondrial granules have been shown to store glycogen, which our staining
303 procedure is particularly well suited to show[56, 57]. Increase of energy storing granules in gametocyte
304 stages could be a plausible preadaptation for survival in the relatively nutrient deprived environment of
305 the mosquito midgut. Alternatively, the EDMGs could represent the mitochondrial RNA granules
306 described in mammalian mitochondria. These are highly proteinaceous, non-membrane delimited sub-
307 compartments in the mitochondrial matrix that are thought to play an important role in mitochondrial
308 RNA processing, mitoribosome assembly, and gene expression[58]. As mitochondrial translation in
309 *Plasmodium* purely relates to complex III and complex IV components of the respiratory chain, this could
310 explain the discrepancy in EDMG size between the comparatively respiratory chain-poor ABS compared
311 to the respiratory chain-rich gametocytes[20, 59].

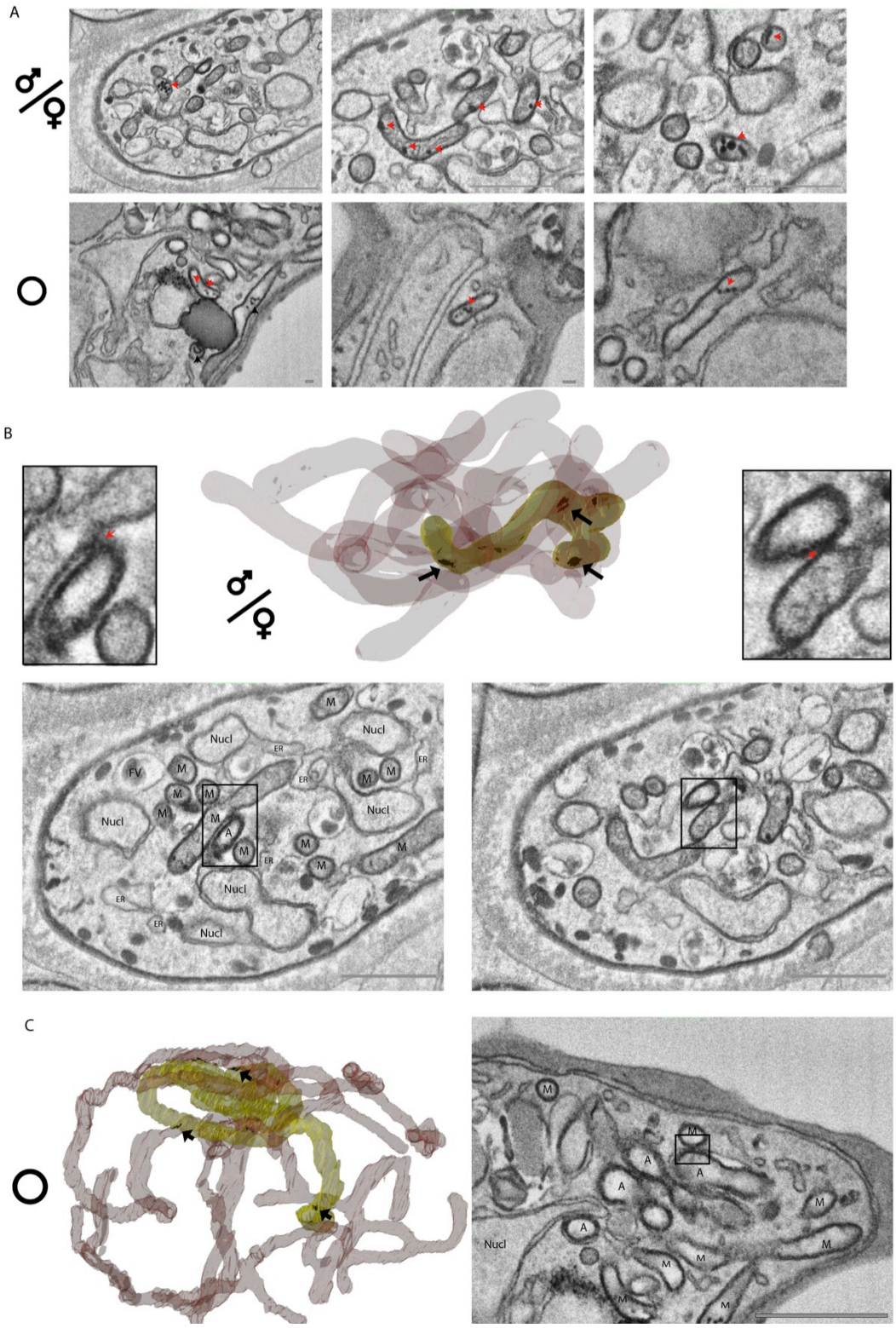

Figure 4 | **Mitochondrial vesicles and interaction with the apicoplast.**
A. Representative micrographs of EDMVs in gametocytes (upper panel, scale bars = 1 µm) and asexual blood stages (lower panel, scale bars = 0.1 µm). Arrowheads highlight examples of EDMVs. **B.** Rendering of exemplary gametocyte mitochondrion (red, high transparency) and apicoplast (yellow, low transparency) with putative organelle interfaces rendered in black. Representative micrographs for two interfaces and respective zoomed crops are shown below. Scale bars = 1 µm. **C.** Same representation as panel B for a schizont. M = Mitochondrion; ER = Endoplasmic reticulum; Nucl = Nucleus; FV = Food vacuole.

319 **Multiple mitochondria in disguise**

320 The current consensus is that, like ABS, gametocytes contain a single heavily branched mitochondrion
321 with diverse morphology that does not closely correspond to gametocyte sex or maturity[19]. Hence, we
322 were surprised to find that while branched and clustered, we did not encounter a fully interconnected
323 mitochondrion in our imaged gametocytes. Instead, we found multiple mitochondria (5-10) per cell that,
324 while clustered and with close membrane appositions, did not share a continuous lumen (Fig. 5A-B,
325 Movies S5-6). To investigate this further, we carefully revisited mitochondrial morphology of a larger
326 number of mature gametocytes using fluorescence microscopy. As expected, most images gave the
327 impression of a fully interconnected organelle, but we also found examples where at least some
328 mitochondrial staining appeared separate from the major cluster (Fig. 5C, Movies S7-10). This is
329 consistent with the FIB-SEM data, where completely separated mitochondria can be observed
330 (Fig. S11A), though in most cases the mitochondria are in close proximity, potentially even suggestive of
331 homotypic membrane interactions that are commonplace among fungal and mammalian mitochondria[60]
332 (Fig. 5B). These short distances of <50nm are well below the diffraction limit of conventional
333 fluorescence microscopy and would appear as a continuous organelle. We observed no morphological
334 indications for poor gametocyte health, which was confirmed by normal gamete activation and the
335 ability of male exflagellation. Moreover, exflagellating males have clearly distinct, dispersed, and
336 rounded mitochondria (Fig. 5D, Movies S11-12). In our FIB-SEM data, we identified one comparable
337 example of a male gametocyte showing bloated, rounded, and dispersed mitochondria that appeared to
338 be in the process of separating, though at this point it is unclear whether this is a male gametocyte at
339 the onset of activation or an aberrant cell (Fig. S11B). We find occasional mature male gametocytes
340 showing a similar pattern using fluorescence microscopy (Fig. S11C). Generally, cristae appeared
341 homogenous across the multiple mitochondria within a gametocyte and were also observed in the
342 bloated and dispersed phenotype (Fig. S11B,D). In comparison, the asexual schizont possesses a single
343 mitochondrion with a continuous lumen, consistent with previous observations, suggesting that the
344 observed phenotype is not directly caused by fixation or sample processing (Fig. 1C)[13]. Taken together,
345 we find consistent evidence for deviation from the current consensus of a fully interconnected
346 mitochondrion in gametocytes. The functional significance of this deviation and appearance in other
347 strains and culturing systems remain to be investigated.

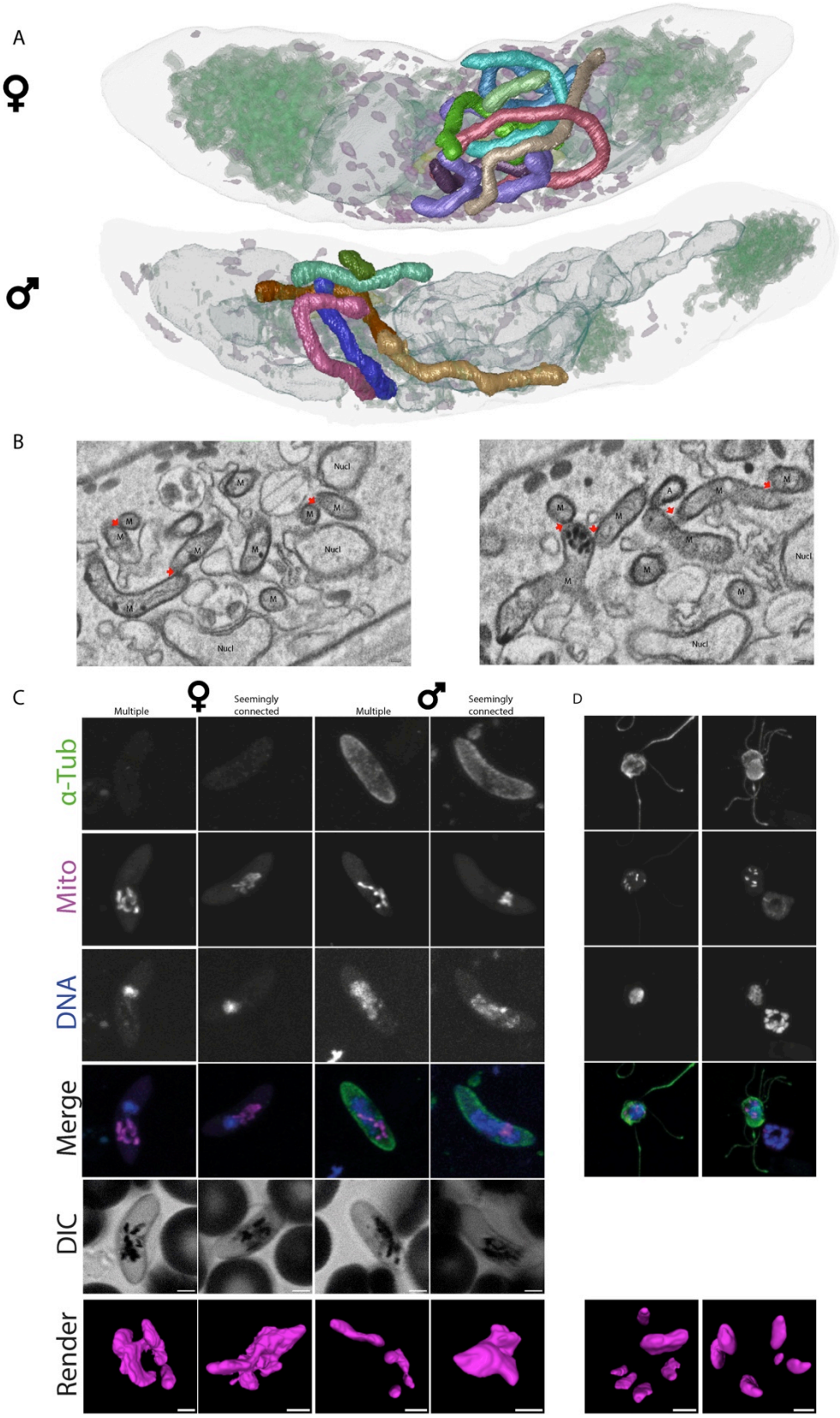

348

349 *Figure 5* | **Gametocytes contain multiple mitochondria in close vicinity.**
350 **A.** Rendering of mature female (upper panel) and male gametocyte (lower panel). Each mitochondrion is rendered in a separate

351 color. The male gametocyte has six distinct mitochondria while the female gametocyte has nine distinct mitochondria. In the
352 female gametocyte membrane appositions are more frequent and mitochondria are more closely associated. Nucleus,
353 osmiophilic bodies, ER, Golgi, and apicoplast are rendered with high transparency to provide cellular context. **B**. Exemplary
354 micrographs showcasing membrane apposition between different mitochondria indicated by red arrows. The mitochondrial
355 membrane remains intact at these sites and no continuity between the different mitochondria is evident. Scale bar = 0.1 µm. M
356 = Mitochondrion; A = Apicoplast; Nucl = Nucleus. **C.** Immunofluorescence analysis of mature and female gametocytes. Depicted
357 left to right are maximum intensity projections using anti-α-tubulin antibodies, MitoTracker™, DAPI, merge of all channels and
358 differential interference contrast (DIC) images. α-tubulin was used to distinguish male and female gametocytes, DNA was
359 visualized using DAPI and mitochondria were visualized using MitoTracker™. For each gender one example was given for
360 recognizably separate mitochondria and a seemingly interconnected mitochondrion. Scale bar = 2 µm Additional renderings of
361 the mitochondrion were generated based on the mitochondrial fluorescence signal (bottom row, scalebar = 1 µm). **D.**
362 Immunofluorescence analysis of exflagellating male gametes. Channels are the same as in **C.** Mitochondria are clearly separate
363 and dispersed throughout the cell body.

364 **Appositions of mitochondrion and apicoplast**

365 In gametocytes, the mitochondria form a network that is wrapped around the apicoplast (Fig. 1 A-B,
366 Movies S1-2). The apicoplast is recognizable as a clearly distinct structure from the mitochondrion due
367 to the thicker appearance of its four surrounding membranes and lack of internal membranous
368 structures and more electron lucent lumen. The mitochondrial-apicoplast network is not spread
369 throughout the whole cell but localized to a relatively central area of the gametocyte, always adjacent to
370 the nucleus. It is noteworthy that this association and the mitochondrial network are much tighter than
371 what we observe in schizonts where the mitochondrion permeates the whole cell (Fig. 1C, Movie S3).
372 The tight association is clearly distinct from the spatial separation of these organelles in sporozoites but
373 akin to the tight association that has been observed in liver-stage parasites[61, 62]. Next to a general vicinity
374 of the two organelles, we observe electron dense junctions spanning the membranes of the two
375 organelles in both gametocyte and ABS (Fig. 4B-C). While it remains unresolved whether these sites
376 constitute a true MCS (Information Box 1), the thickened electron dense interaction area is indicative of
377 a tethering structure, providing a reasonable explanation why the organelles are consistently co-
378 purified[63]. While a putative physical connection does not provide mechanistic evidence, the observed
379 phenomenon may facilitate metabolic cooperation, *e.g.* by serving as an exchange site for metabolites
380 of the heme biosynthesis pathway for which the enzymes are localized partly in the mitochondrion and
381 partly in the apicoplast[64, 65].

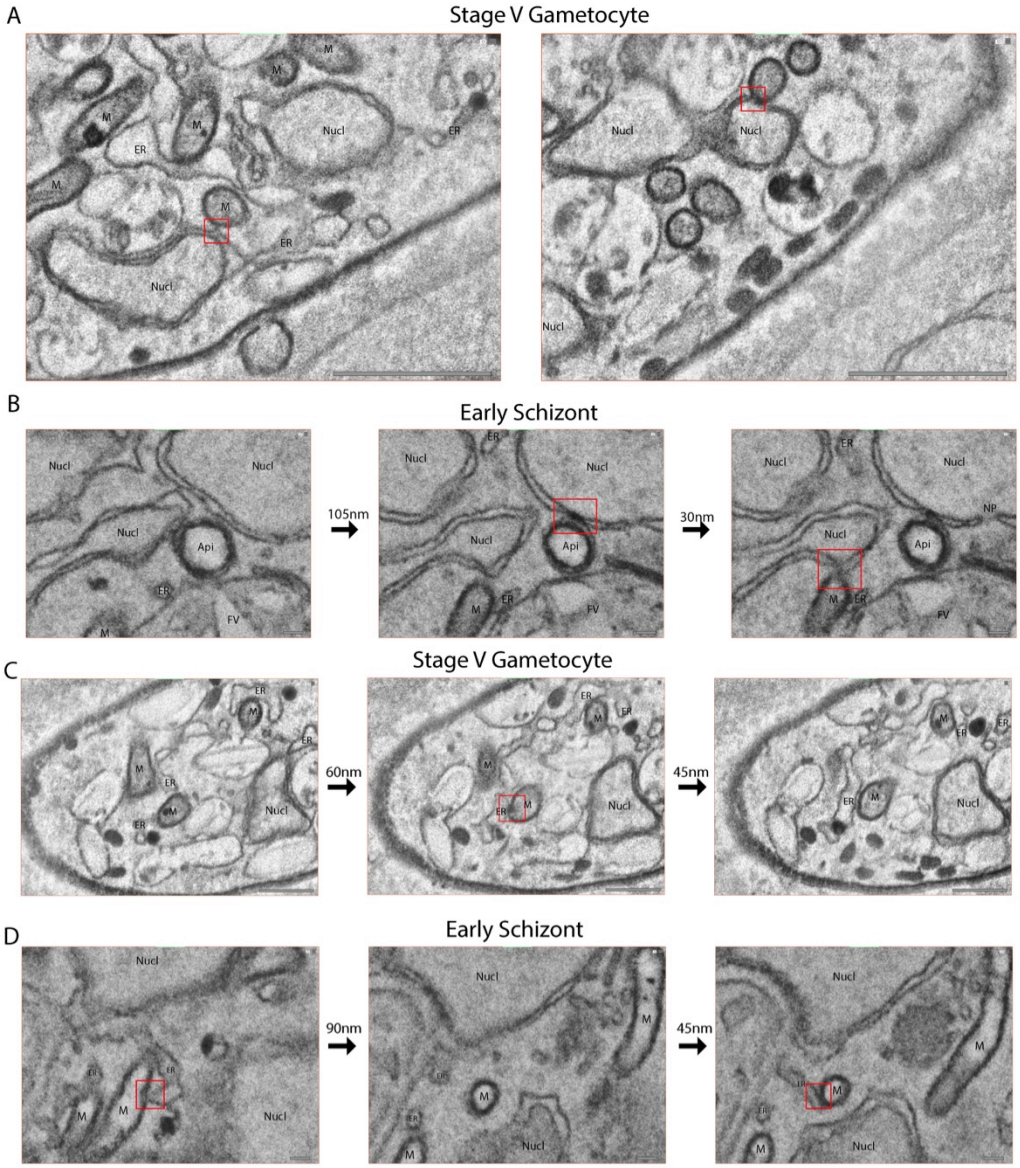

Figure 6 | **Putative organelle interfaces in blood stages.**
A. Representative micrographs showing putative mitochondrion-nucleus interaction sites in a mature gametocyte. The respective sites are highlighted through a red box. Scale bars = 1 µm. **B.** Representative series of micrographs showing putative mitochondrion-nucleus and apicoplast-nucleus interaction sites in a schizont. The three frames are crops at the same x,y-coordinates in the acquisition plane but are at different z-depth with the respective distance displayed between micrographs. **C.** As in (B), showing putative mitochondrion-ER interaction sites in a mature gametocyte. Scale bars = 1 µm. **D.** As in (B), showing putative mitochondrion-ER interaction sites in a schizont. Scale bars = 0.1 µm M = Mitochondrion; ER = Endoplasmic reticulum; Nucl = Nucleus; FV = Food vacuole.

Appositions of ER and mitochondrion

From mammalian and yeast mitochondria, we know that the ER is intimately linked to and interacts with the mitochondrion through MCS. In these species, MCS cover 2-5% of the mitochondrial surface area and are composed of a known set of interactive proteins[66, 67]. These sites are thought to be crucial for lipid homeostasis and calcium transport. In our data, we similarly find multiple sites where the ER is in very close proximity to the mitochondrion (Fig. 6C-D). Anecdotally, both in the schizonts and gametocytes, we find examples where these sites are accompanied by EDMGs appearing to span the

398 mitochondrial membrane and contact the ER (Fig. S12), which provides tentative support for a role of
399 EDMGs in calcium storage and/or mobilization. The appearance of the ER-mitochondrion appositions
400 resembles micrographs of previously described ER-mitochondrion MCS[68], leading us to believe that they
401 are conserved in *Plasmodium*. However, from all previously described tethering complexes, the
402 *Plasmodium* genome is lacking at least one critical component[69-72]. In *S. cerevisiae*, the ER membrane
403 complex (EMC) and TOM5 facilitate phospholipid exchange between ER and mitochondrion[73]. Recently,
404 we demonstrated that an assembled EMC is present in *P. falciparum*[20], but a TOM5 orthologue is not
405 encoded in *Plasmodium*. This prompted us to re-interrogate the underlying complexomics data and look
406 for another potential mitochondrial interactor with the EMC. In doing so, we found that *Pf*TOM7,
407 another component of the translocase of the outer membrane (TOM) complex, comigrates in native
408 electrophoresis with the EMC as well as the TOM complex (Fig. S13A). Looking at the multiple sequence
409 alignment, few residues are conserved outside of the transmembrane region and none are shared
410 between *Sc*TOM5 and *Pf*TOM7 (Fig. S13B-C). While overall structural features of *Pf*TOM7 and *Sc*TOM7,
411 based on alignment of the *Pf*TOM7 AlphaFold prediction[74] and experimentally determined structure of
412 *Sc*TOM7[75, 76] appear similar, *Sc*TOM5 is expectedly less similar outside of the (predicted) TM helix
413 (Fig. S13D). This suggests that if *Pf*TOM7, based on comigration with the EMC complex, is a tether, the
414 specific binding site is unlikely to be conserved. If a different mechanism tethers these two complexes, it
415 might also suggest that there is biological utility in specifically facilitating the tether through a
416 component of the TOM complex.

417 **Features and dimorphism of the gametocyte nucleus**

418 The nucleus is bounded by an inner and outer leaflet of the nuclear envelope, where the outer leaflet is
419 continuous with the ER and the inner leaflet circumscribes the nucleus. In gametocytes, we find an
420 intriguing deviation from the typically round or oval nuclear shape[77]. The nuclei share a bulbous body
421 from which thinner diverse extensions extrude predominantly in one direction covering large parts of
422 the cell (Fig. 7A-B). The bulbous body always contains a more electron dense, not membrane-bound
423 region, which has previously been assigned as the nucleolus of the female gametocyte[22] (Fig. 7C). The
424 observed nuclear shapes are largely consistent with prior studies that noted a discrepancy between a
425 relatively small and localized DNA stain and an elongated staining from a nucleus-targeted
426 fluorophore[15, 78]. In stage IV – V gametocytes, a clear nuclear dimorphism is apparent with female
427 gametocytes possessing a less complex smaller nucleus with an average volume of 6.6 ± 0.3 μm^3, while
428 males have a more complex nuclear shape and a much higher nuclear volume at 12.4 ± 1.1 μm^3 (Fig. 7B).
429 A comparatively enlarged nucleus in males is consistent with well-known differences observed in
430 Giemsa-stained samples and might prepare male gametocytes for the rapid nuclear division and DNA
431 replication that they undergo upon activation. While smaller, the female nucleus is still relatively large,
432 possibly explained by the proposed role of the nuclear extension in elongation of the gametocyte[15].
433 Based on our measurements, for merozoites the same genetic material fits into a nucleus of ~0.5 μm^3
434 while for our exemplary schizont in the process of DNA duplication, average nuclear volume is around
435 1.8 μm^3. Stage II - III immature gametocytes also reflect the nuclear dimorphism observed in stage IV – V
436 gametocytes, with some having a relatively smaller and less complex nucleus while another subset has a
437 bigger and more complex nucleus (Fig. 7A). While we cannot confidently assign the developing
438 gametocytes to either gender, a plausible hypothesis would be that the subset with smaller nucleus
439 represents immature female gametocytes, while cells with larger nucleus represent immature male
440 gametocytes. However, this is in conflict with a recent finding that commitment, as indicated by
441 measurable differences in gene expression, to either male or female cell fate is only decided at stage

442 III[79]. Furthermore, a recent study utilizing array tomography has found no such nuclear dimorphism in
443 earlier stages but does show the same similar dimorphism and absolute volumes to our findings for later
444 stages[15]. It would be interesting to see whether these different observations stem from differences in
445 experimental methods, stage assignment, image segmentation or biological material.

446 **Appositions of nucleus and endosymbiotic organelles**

447 In *Plasmodium*, both mitochondrion and apicoplast have essential organellar ribosomes, with promising
448 features as drug targets[80-83]. Nevertheless, neither have an associated set of organelle targeted tRNAs
449 that would be sufficient to facilitate translation of their respective genomes[84]. Recently, it has been
450 found that the nuclear-mitochondrial MCS play a role in RNA exchange and signaling. These sites are
451 distinct from the well-characterized peripheral ER-mitochondrial MCS but likewise enabled by tether
452 proteins without obvious homologues in the *Plasmodium* genome[85, 86]. We find distinct appositions of
453 the nucleus and mitochondrion in both schizonts and gametocytes (Fig. 6A-B). At these sites there
454 appears to be continuity of the outer leaflet of the nuclear envelope and the outer mitochondrial
455 membrane. In contrast, we find that the nucleus-apicoplast interface in ABS is characterized by a local
456 condensation of the normally spatially separated layers of the nuclear envelope into one electron
457 denser layer without obvious membrane fusion (Fig. 6B). Whereas the mitochondrion in gametocytes
458 closely envelops large areas of the apicoplast, only a subset of cells have close physical proximity
459 between nucleus and apicoplast and in those cells we never find indications of direct membrane
460 contact. Functionally, interfaces of apicoplast and mitochondrion with the nucleus might serve
461 phospholipid homeostasis or RNA exchange as has been suggested in model eukaryotes[85, 86], or provide
462 a potential mechanism for import of organellar tRNAs without known targeting signals thus shoring up
463 the incomplete translational machinery in these organelles.

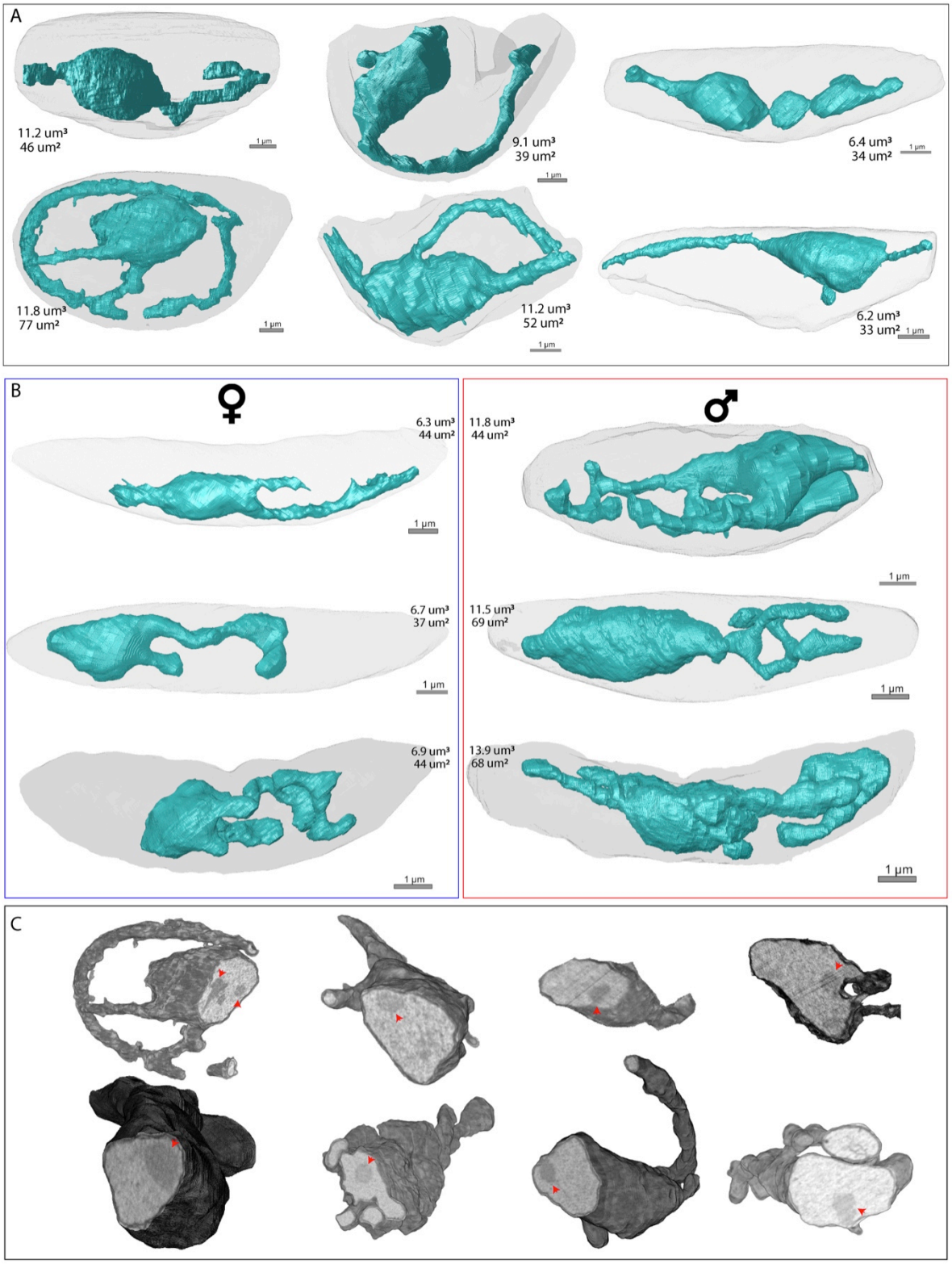

Figure 7 | **Distinct nuclear morphology in gametocytes.**
Renderings of nuclei (teal) in (**A**) stage II-III and (**B**) stage IV-V gametocytes. Stage IV/V gametocytes are divided in female (blue outline) and male (red outline) gametocytes based on the number and appearance of osmiophilic bodies, hemozoin distribution and ER prevalence. For all nuclei, the respective volumes and surface areas are indicated. **C.** Rendering of cross section of nuclei with gray values from EM data overlaid. Red arrowheads point at the position of the putative nucleolus.

470 **Conclusion & Future Outlook**

471 In this study, we applied volumetric electron microscopy to the transmittable gametocyte stages of the
472 malaria parasite, allowing us to place findings from the past into their current molecular context and
473 tackle questions that are challenging to address using single sections or serial sections with low z-
474 resolution such as the connectivity within or between various organelles. Furthermore, these data
475 allowed us to create the first 3D visualization of Golgi, gametocyte cytostome, Garnham body, and ER in
476 gametocytes, improving our understanding of the cellular architecture in this part of the life cycle. In
477 doing so, we are aware of the descriptive nature of this study and the limitations of the tool applied. Any
478 of the hypotheses put forward are meant to provide a foundation for controlled molecular studies and
479 targeted approaches that are more suitable to identify the underlying molecular players.

480 **Public access and potential for reusability**

481 FIB-SEM is a powerful tool, particularly for a cellular system that is as unusual as malaria parasites, as it
482 allows determination of general ultrastructural organization and basic measurements to cover
483 knowledge gaps that in other model eukaryotes have long been closed. Similar to other global datasets,
484 one of the biggest challenges is to extract all relevant information and leverage the utility of non-
485 targeted approaches and not just use them to answer one narrow question. To facilitate future re-
486 interrogation of the data, we have deposited all underlying image stacks, as well as all analyzed cells and
487 their corresponding segmentations, in the Electron Microscopy Public Image Archive (EMPIAR-11497).
488 We hope that the latter can serve as training data for machine learning by groups with more suitable
489 hardware/software and deep learning expertise to greatly simplify annotation workflows in the future.

Textbox 1 Membrane contact sites

Membrane contact sites (MCS) have typically been defined as areas of membranes of two organelles that are in close proximity to each other. These areas can be homotypic (between the same type of organelle, e.g. mitochondrion-mitochondrion MCS) or heterotypic (between different organelle types, e.g. mitochondrion-ER MCS). To increase clarity and create a unified vocabulary Scorrano *et al.*[87] have put together a set of unifying features that a MCS should have to be characterized as such.

1. There should be tethering forces from either protein-lipid or protein-protein interactions that maintain the distance. This replaces previous proximity ranges that were used as guidelines as contact sites have been found that far exceed these distance guidelines.

2. There should be no fusion of membranes. If there is fusion of membranes this can be referred to as docking or fusion. Vesicular transport at the contact site may exist within this definition.

3. All contact sites should fulfill a specific function. A disruption of a contact site should impact cell function.

4. MCS should have a defined proteome or lipidome that is required for their function, maintenance, or regulation.

5. Time is not a factor. Dynamic or transient structures that fulfill the other requirements can be considered a MCS.

490

491 **Materials & Methods**

492 **Parasite culture & gametocyte induction**

493 All parasite material used in this study is derived from the NF54/iGP2 strain. NF54/iGP2 parasites were
494 previously shown to be able successfully complete the whole lifecycle as well as not markedly differ
495 from wildtype NF54 parasites in other parameters that were investigated[78]. This parasite strain has the
496 desirable property that gametocytogenesis can be selectively induced by removal of glucosamine from
497 the medium, which triggers sexual commitment through the transcriptional cascade centered around
498 the AP2G gene[88]. Asexual blood-stage parasites (ABS) were maintained according to standard culturing
499 procedure in RPMI [7.4] supplemented with 10% human serum and 5% hematocrit using standard
500 culturing technique in a semi-automatic culturing system[5, 89]. For the maintenance of the NF54/iGP2
501 strain, an additional supplement of 2.5 mM D-(+)-glucosamine hydrochloride (Sigma #1514) was used.
502 To induce gametocytogenesis, glucosamine was omitted from the culturing medium. Between days 4
503 and 8 after gametocyte induction 50 mM N-acetylglucosamine (Sigma #A6525) was used to eliminate
504 ABS parasites. On day 14 gametocyte-infected RBCs were separated from uninfected RBCs through
505 magnetic separation as described previously[90]. Close attention was paid to prewarm and maintain all
506 solutions and apparatus at 37°C to avoid unintended activation of mature gametocytes. As reference
507 material trophozoite and schizont stages from mixed ABS cultures were similarly enriched through
508 magnetic separation and processed alongside the gametocyte cultures. For sample 3, N-
509 acetylglucosamine treatment was omitted to control for phenotypes causes by this treatment. This
510 omission leads to presence of ABS in the resulting images (sample 3).

511 **Sample preparation for electron microscopy**

512 Samples were prepared as described previously[20]. Briefly, the enriched infected red blood cells were
513 fixed using 2% glutaraldehyde in 0.1 M cacodylate (pH 7.4) buffer overnight at a temperature of 4 °C.
514 The fixed cells were then washed and the cell-pellet was resuspended in 3% ultra-low-gelling agarose,
515 solidified, and cut into small blocks. The agarose blocks containing the fixed cells were postfixed for
516 1 hour at room temperature using a solution of 2% osmium tetroxide and 1.5% potassium ferrocyanide
517 in 0.1 M cacodylate buffer containing 2 mM CaCl2, washed in MQ and then treated with 0.5%
518 thiocarbohydrazide for 30 minutes at room temperature. After washing, the agarose blocks were again
519 suspended in 2% osmium for 30 minutes at room temperature, washed, and then placed in a 2%
520 aqueous uranyl acetate solution overnight at 4 °C. The blocks were then washed and placed in a lead
521 aspartate solution (pH 5.5) for 30 minutes at 60 °C, washed, dehydrated using an ascending series of
522 aqueous ethanol solutions, and subsequently transferred via a mixture of acetone and Durcupan to pure
523 Durcupan (Sigma) as an embedding medium. The aforementioned staining procedure is primarily
524 optimized for high membrane contrast and staining of lipid-rich structures due by utilizing the
525 combination of potassium ferrocyanide, osmium tetroxide and thiocarbohydrazide[91]. Uranyl acetate and
526 lead aspartate furthermore stain DNA/RNA, proteins as well as carbohydrates[92, 93].

527 **FIB-SEM**

528 After polymerization and in order to create a smooth plane for FIB-SEM imaging, the sample surface was
529 smoothened using an ultra-microtome (Reichert Ultracut S ultramicrotome (Leica microsystems)). The
530 region of interest was cut out of the resin block and glued on an SEM stub with carbon tape, using
531 conductive silver paint. The samples were then coated with a gold sputter coater (Edwards, Stockholm,
532 Sweden) before introduction into a Zeiss Crossbeam 550 FIB-SEM (Carl Zeiss).
533 Multiple coarse trenches were milled using a 30 kV@30 nA probe to choose the regions of interest for
534 further 3D volume imaging. Parameters for serial sectioning imaging of large regions were set using the

535 Atlas 3D software (Atlas Engine v5.3.3). The large trenches were first smoothened using a 30 kV@1.5 nA
536 FIB probe, and thereafter a 30 kV@700 pA probe current was used for serial FIB milling. InLens
537 secondary and backscattered electron microscopy images were simultaneously collected at an
538 acceleration voltage of 2.0 kV with a probe current of 500 pA. The backscattered grid was set to −902 V.
539 For noise reduction, images were acquired using line average (n=1) and a dwell time of 3,0 µs. The
540 milling and imaging processes were continuously repeated and long series of images were acquired.
541

	Sample 1	Sample 2	Sample 3	Sample 4	Sample 5
Life-cycle stage	GCT	GCT	GCT w/ ABS	ABS	ABS
Dimensions (x,y,z) [nm]	4268x2784x2293	4428x3804x952	4402x2850x900	4423x1430 x 1085	4010x3157x739
Total Volume Imaged [um^3]	10217	6013	4234	2573	3508

542 Table 1. Basic parameters of FIB-SEM stacks used in these studies. All samples constitute biological replicates.
543

544 **Serial sectioning**

545 To have a lower noise reference and identify potential FIB imaging artifacts one gametocyte sample was
546 also analyzed through serial sectioning combined with SEM. After checking for desired density of cells
547 with toluidine blue corresponding resin block was trimmed to the desired size and mounted onto the
548 chuck of a Leica Artos 3D Ultramicrotome. The block was sectioned into thin 80nm slices and sections
549 were collected onto Indium Tin Oxide glass coated with 5 nm carbon. The sections were then imaged
550 with a scanning electron microscope (Sigma300, Zeiss) at an acceleration voltage of 30 kV (HDBSD, 60
551 µm, high current) using Atlas 5 software. In total 47 consecutive images were taken leading to a total
552 imaged volume of 15124 um^3.
553

554 **Post-processing and segmentation**

555 All processing, visualization and analysis performed in the ORS Dragonfly software (V2022.2).
556 Wherever necessary image stacks were aligned using the mutual information and sum of squared
557 differences registration method and results were manually controlled and adjusted whenever necessary.
558 Contrast was enhanced through application of contrast limited adaptive histogram equalization (CLAHE).
559 3D segmentation was performed using either manual segmentation or deep learning based
560 segmentation, based on which cellular feature was segmented. Deep-learning based segmentations
561 were controlled for errors and manually adjusted when necessary. For 3D rendering the segmented
562 regions of interest were converted to triangle meshes.

563 **Immunofluorescence assays**

564 To induce gametocytes, NF54 parasites were swapped from their earlier described complete culture
565 media to RPMI media supplemented with 0.5% Albumax (AlbuMAX II™, Thermo Fisher, #11021-037) at
566 26 hours post invasion. The parasites were allowed to commit for 36 hours, before being put back on
567 complete culture media. At day 12 post induction, stage V gametocytes were stained in 100 nM
568 MitoTracker™ (MitoTracker™ Orange CMTMRos, Thermo Fisher, #M7510) diluted in complete media at
569 37°C for 30 minutes. Stage V gametocyte samples were diluted 1:10 in warm complete media before
570 being allowed to settle on pre-heated Poly-L-Lysine coated coverslips (Corning, #354085) for 15 minutes
571 at 37°C, while activated gamete samples were mixed 1:1 with in 30µM xanthurenic acid (Sigma Aldrich,
572 #D120804) and subsequently settled for 15 minutes at RT. Both samples were fixed with 4%
573 paraformaldehyde (Thermo Fisher, #28906)) and 0.0075% glutaraldehyde (Panreac, #A0589,0010) in
574 PBS for 20 minutes at RT. The fixed samples were, permeabilised with 0.1% Triton X-100 in PBS for 10
575 minutes and blocked in 3% BSA (Sigma Aldrich, #A9418) for 1 hour at RT. To differentiate between male
576 and female gametocytes, the samples were stained with primary α-Tubulin antibody (Thermo Fisher,
577 #MA1-19162) for 1 hour at RT, which was visualised with Donkey anti-Mouse Alexa Fluor™ 647 (Thermo

Fisher, #A-31571). Finally, samples were stained with 300 nM DAPI (Thermo Fisher, #62248) for 30 minutes at RT before being mounted on a microscope slide using VECTASHIELD (VWR, #H-1000) and sealed in nail polish. The samples were imaged on an confocal LSM900 microscope with airyscan (Zeiss). Z-stack images were obtained with a 0.14 µm step size. Laser power and detector sensibility are maintained the same throughout all the images. A maximum projection was created for every image, in which the tubulin signal was pre-set in order to differentiate between male and female gametocytes.

Acknowledgements

We thank the molecular team members of the Malaria Research Group for fruitful discussions. We also thank Nico Sommerdijk and the Radboud Technology Center Microscopy - Electron Microscopy Center for supporting this work and Sabrina Absalon for critically proofreading the manuscript. F.E. and T.W.A.K. were supported by the Netherlands Organisation for Scientific Research (NWO-VIDI 864.13.009), C.B. by a PhD fellowship from the Radboud Institute for Molecular Life Sciences, Radboudumc (RIMLS018-009b), J.M.J.V. was supported by an individual Radboudumc Master-PhD grant. R.R. and A.A. are supported by an ERC Advanced Investigator grant (H2020-ERC-2017-ADV-788982-COLMIN for Nico Sommerdijk). A.A. is also supported by the NWO (VI.Veni.192.094).

Author contributions

F.E., R.R, C.B., M.K.L and J.M.J.V. performed experiments. R.E.S provided conceptual advice and analysis. F.E. analyzed the results, prepared illustrations and wrote the manuscript draft. A.A. provided resources technical expertise and conceptual advice. T.W.A.K. contributed to conceptual development, provided resources and edited the manuscript. All authors contributed to data interpretation and provided feedback on the manuscript. All authors approved the final version of the manuscript.

Literature

1. World Health, O. World malaria report 2021. (World Health Organization, Geneva; 2021).
2. Organization, W.H. World malaria report 2022. (World Health Organization, 2022).
3. Monroe, A., Williams, N.A., Ogoma, S., Karema, C. & Okumu, F. Reflections on the 2021 World Malaria Report and the future of malaria control. *Malaria Journal* **21**, 154 (2022).
4. Munro, B.A. & McMorran, B.J. in Parasitologia, Vol. 2 101-124 (2022).
5. Ponnudurai, T., Lensen, A.H.W., Meis, J.F.G.M. & Meuwissen, J.H.E.T. Synchronization of *Plasmodium falciparum* gametocytes using an automated suspension culture system. *Parasitology* **93**, 263-274 (1986).
6. Sinden, R.E., Canning, E.U., Bray, R.S., Smalley, M.E. & Garnham, P.C.C. Gametocyte and gamete development in *Plasmodium falciparum*. *Proc R Soc Lond B Biol Sci* **201**, 375-399 (1978).
7. Langreth, S.G. Electron microscope cytochemistry of host-parasite membrane interactions in malaria. *Bull World Health Organ* **55**, 171-178 (1977).
8. Kass, L., Willerson, D., Rieckmann, K., Carson, P. & Becker, R. *Plasmodium falciparum* Gametocytes: Electron Microscopic Observations on Material Obtained by a New Method. *The American journal of tropical medicine and hygiene* **20**, 187-194 (1971).
9. Bannister, L.H., Hopkins, J.M., Fowler, R.E., Krishna, S. & Mitchell, G.H. Ultrastructure of rhoptry development in *Plasmodium falciparum* erythrocytic schizonts. *Parasitology* **121**, 273-287 (2000).
10. Bannister, L.H., Hopkins, J.M., Margos, G., Dluzewski, A.R. & Mitchell, G.H. Three-Dimensional Ultrastructure of the Ring Stage of *Plasmodium falciparum*: Evidence for Export Pathways. *Microscopy and Microanalysis* **10**, 551-562 (2004).

621 11. Sinden, R.E. & Strong, K. An ultrastructural study of the sporogonic development of *Plasmodium*
622 *falciparum* in Anopheles gambiae. *Trans R Soc Trop Med Hyg* **72**, 477-491 (1978).
623 12. Slomianny, C., Prensier, G. & Charet, P. Ingestion of erythrocytic stroma by *Plasmodium*
624 *chabaudi* trophozoites: ultrastructural study by serial sectioning and 3-dimensional
625 reconstruction. *Parasitology* **90 (Pt 3)**, 579-588 (1985).
626 13. Rudlaff, R.M., Kraemer, S., Marshman, J. & Dvorin, J.D. Three-dimensional ultrastructure of
627 *Plasmodium falciparum* throughout cytokinesis. *PLOS Pathogens* **16**, e1008587 (2020).
628 14. Araki, T. *et al.* Three-dimensional electron microscopy analysis reveals endopolygeny-like
629 nuclear architecture segregation in *Plasmodium*oocyst development. *Parasitology International*
630 **76**, 102034 (2020).
631 15. Li, J. *et al.* Repurposing the mitotic machinery to drive cellular elongation and chromatin
632 reorganisation in *Plasmodium falciparum* gametocytes. *Nature Communications* **13**, 5054
633 (2022).
634 16. Parkyn Schneider, M. *et al.* Disrupting assembly of the inner membrane complex blocks
635 *Plasmodium falciparum* sexual stage development. *PLoS Pathog* **13**, e1006659 (2017).
636 17. Rashpa, R. & Brochet, M. Expansion microscopy of *Plasmodium*gametocytes reveals the
637 molecular architecture of a bipartite microtubule organisation centre coordinating mitosis with
638 axoneme assembly. *PLOS Pathogens* **18**, e1010223 (2022).
639 18. Matz, J.M., Goosmann, C., Matuschewski, K. & Kooij, T.W.A. An Unusual Prohibitin Regulates
640 Malaria Parasite Mitochondrial Membrane Potential. *Cell Reports* **23**, 756-767 (2018).
641 19. Okamoto, N., Spurck Timothy, P., Goodman Christopher, D. & McFadden Geoffrey, I. Apicoplast
642 and Mitochondrion in Gametocytogenesis of *Plasmodium falciparum*. *Eukaryotic Cell* **8**, 128-132
643 (2009).
644 20. Evers, F. *et al.* Composition and stage dynamics of mitochondrial complexes in *Plasmodium*
645 *falciparum*. *Nat Commun* **12**, 3820 (2021).
646 21. Krungkrai, S.R., Learngaramkul, P., Kudan, S., Prapunwattana, P. & Krungkrai, J. Mitochondrial
647 heterogeneity in human malarial parasite *Plasmodium falciparum*. *Science Asia* **25**, 77-83 (1999).
648 22. Sinden, R.E. Gametocytogenesis of *Plasmodium falciparum* in vitro: an electron microscopic
649 study. *Parasitology* **84**, 1-11 (1982).
650 23. de Koning-Ward, T.F. *et al.* The role of osmiophilic bodies and Pfg377 expression in female
651 gametocyte emergence and mosquito infectivity in the human malaria parasite *Plasmodium*
652 *falciparum*. *Mol Microbiol* **67**, 278-290 (2008).
653 24. Olivieri, A. *et al.* Distinct properties of the egress-related osmiophilic bodies in male and female
654 gametocytes of the rodent malaria parasite *Plasmodium berghei*. *Cell Microbiol* **17**, 355-368
655 (2015).
656 25. Aikawa, M., Huff, C.G. & Sprinz, H. Comparative fine structure study of the gametocytes of avian,
657 reptilian, and mammalian malarial parasites. *J Ultrastruc Res* **26**, 316-331 (1969).
658 26. Sassmannshausen, J. *et al.* Comparative proteomics of vesicles essential for the egress of
659 *Plasmodium falciparum* gametocytes from red blood cells. *bioRxiv*, 2023.2002.2008.527640
660 (2023).
661 27. Liu, B. *et al.* Multimodal analysis of *Plasmodium knowlesi*-infected erythrocytes reveals large
662 invaginations, swelling of the host cell, and rheological defects. *Cell Microbiol* **21**, e13005 (2019).
663 28. Garnham, P.C.C. Malaria parasites and other Haemosporidia. *Malaria Parasites and other*
664 *Haemosporidia.* (1966).
665 29. Petter, M., Bonow, I. & Klinkert, M.-Q. Diverse Expression Patterns of Subgroups of the rif
666 Multigene Family during *Plasmodium falciparum* Gametocytogenesis. *PLOS ONE* **3**, e3779
667 (2008).

668 30. Garnham, P. On Some Curious Bodies found in Erythrocytes containing Immature Crescents.
669 *Transactions of the Royal Society of Tropical Medicine and Hygiene* **26** (1933).
670 31. Orjih, A.U. Hemozoin accumulation in Garnham bodies of *Plasmodium falciparum* gametocytes.
671 *Parasitology Research* **111**, 2353-2359 (2012).
672 32. Raventos-Suarez, C., Kaul, D.K., Macaluso, F. & Nagel, R.L. Membrane knobs are required for the
673 microcirculatory obstruction induced by *Plasmodium falciparum*-infected erythrocytes.
674 *Proceedings of the National Academy of Sciences* **82**, 3829-3833 (1985).
675 33. Quadt, K.A. *et al.* The density of knobs on *Plasmodium falciparum*-infected erythrocytes
676 depends on developmental age and varies among isolates. *PLoS One* **7**, e45658 (2012).
677 34. Milani, K.J., Schneider, T.G. & Taraschi, T.F. Defining the morphology and mechanism of the
678 hemoglobin transport pathway in *Plasmodium falciparum*-infected erythrocytes. *Eukaryot Cell*
679 **14**, 415-426 (2015).
680 35. Xie, S.C., Ralph, S.A. & Tilley, L. K13, the Cytostome, and Artemisinin Resistance. *Trends in*
681 *Parasitology* **36**, 533-544 (2020).
682 36. Tran, P.N. *et al.* Changes in lipid composition during sexual development of the malaria parasite
683 *Plasmodium falciparum*. *Malar J* **15**, 73 (2016).
684 37. Mathur, J., Kroeker, O.F., Lobbezoo, M. & Mathur, N. The ER Is a Common Mediator for the
685 Behavior and Interactions of Other Organelles. *Frontiers in Plant Science* **13** (2022).
686 38. Khan, S.M. *et al.* Proteome Analysis of Separated Male and Female Gametocytes Reveals Novel
687 Sex-Specific *Plasmodium*Biology. *Cell* **121**, 675-687 (2005).
688 39. Janse, C. & Waters, A. Sexual development of malaria parasites. (Norwich: Horizon Scientific
689 Press, 2004).
690 40. Adisa, A. *et al.* Re-assessing the locations of components of the classical vesicle-mediated
691 trafficking machinery in transfected *Plasmodium falciparum*. *Int J Parasitol* **37**, 1127-1141
692 (2007).
693 41. Krai, P., Dalal, S. & Klemba, M. Evidence for a Golgi-to-Endosome Protein Sorting Pathway in
694 *Plasmodium falciparum*. *PLOS ONE* **9**, e89771 (2014).
695 42. Hallée, S. *et al.* Identification of a Golgi apparatus protein complex important for the asexual
696 erythrocytic cycle of the malaria parasite *Plasmodium falciparum*. *Cell Microbiol* **20**, e12843
697 (2018).
698 43. Jonsdottir, T.K., Gabriela, M., Crabb, B.S., F. de Koning-Ward, T. & Gilson, P.R. Defining the
699 Essential Exportome of the Malaria Parasite. *Trends in Parasitology* **37**, 664-675 (2021).
700 44. Alano, P. *Plasmodium falciparum* gametocytes: still many secrets of a hidden life. *Molecular*
701 *Microbiology* **66**, 291-302 (2007).
702 45. Tibúrcio, M. *et al.* Early gametocytes of the malaria parasite *Plasmodium falciparum* specifically
703 remodel the adhesive properties of infected erythrocyte surface. *Cell Microbiol* **15**, 647-659
704 (2013).
705 46. Beck, J., Muralidharan, V., Oksman, A. & Goldberg, D. PTEX component HSP101 mediates export
706 of diverse malaria effectors into host erythrocytes. *Nature* **511** (2014).
707 47. Jennison, C. *et al.* Inhibition of Plasmepsin V Activity Blocks *Plasmodium falciparum*
708 Gametocytogenesis and Transmission to Mosquitoes. *Cell Reports* **29**, 3796-3806.e3794 (2019).
709 48. Matthews, K. *et al.* The *Plasmodium*translocon of exported proteins (PTEX) component
710 thioredoxin-2 is important for maintaining normal blood-stage growth. *Mol Microbiol* **89**, 1167-
711 1186 (2013).
712 49. Ngotho, P. *et al.* Revisiting gametocyte biology in malaria parasites. *FEMS Microbiol Rev* **43**, 401-
713 414 (2019).
714 50. Dearnley, M.K. *et al.* Origin, composition, organization and function of the inner membrane
715 complex of *Plasmodium falciparum* gametocytes. *J Cell Sci* **125**, 2053-2063 (2012).

716 51. Mühleip, A. *et al.* ATP synthase hexamer assemblies shape cristae of Toxoplasma mitochondria.
717 *Nature Communications* **12**, 120 (2021).
718 52. Hanssen, E., Goldie, K.N. & Tilley, L. Ultrastructure of the asexual blood stages of *Plasmodium*
719 *falciparum*. *Methods Cell Biol* **96**, 93-116 (2010).
720 53. Evers, F. *et al.* Composition and stage dynamics of mitochondrial complexes in *Plasmodium*
721 *falciparum*. *Nature Communications* **12**, 3820 (2021).
722 54. Uyemura, S.A., Luo, S., Moreno, S.N. & Docampo, R. Oxidative phosphorylation, Ca2+ transport,
723 and fatty acid-induced uncoupling in malaria parasites mitochondria. *Journal of Biological*
724 *Chemistry* **275**, 9709-9715 (2000).
725 55. Wolf, S.G. *et al.* 3D visualization of mitochondrial solid-phase calcium stores in whole cells. *Elife*
726 **6** (2017).
727 56. Goldfischer, S., Kress, Y., Coltoff-Schiller, B. & Berman, J. Primary fixation in osmium-potassium
728 ferrocyanide: the staining of glycogen, glycoproteins, elastin, an intranuclear reticular structure,
729 and intercisternal trabeculae. *J Histochem Cytochem* **29**, 1105-1111 (1981).
730 57. Kacem, H., Giese, E.G. & Miquel, J. Sperm characters in the Hemiuridae (Digenea): first data on
731 Aphanurus stossichii (Aphanurinae) and Ectenurus lepidus (Dinurinae). *Parasitology Research*
732 **119**, 991-999 (2020).
733 58. Rey, T. *et al.* Mitochondrial RNA granules are fluid condensates positioned by membrane
734 dynamics. *Nature Cell Biology* **22**, 1180-1186 (2020).
735 59. Atkinson, A. & Winge, D.R. Metal Acquisition and Availability in the Mitochondria. *Chemical*
736 *Reviews* **109**, 4708-4721 (2009).
737 60. Cohen, M.M. & Tareste, D. Recent insights into the structure and function of Mitofusins in
738 mitochondrial fusion. *F1000Research* **7** (2018).
739 61. Kudryashev, M. *et al.* Positioning of large organelles by a membrane-associated cytoskeleton in
740 *Plasmodium*sporozoites. *Cellular microbiology* **12**, 362-371 (2010).
741 62. Stanway, R.R. *et al.* Organelle segregation into *Plasmodium*liver stage merozoites. *Cellular*
742 *Microbiology* **13**, 1768-1782 (2011).
743 63. Kobayashi, T. *et al.* Mitochondria and apicoplast of *Plasmodium falciparum*: behaviour on
744 subcellular fractionation and the implication. *Mitochondrion* **7**, 125-132 (2007).
745 64. Sato, S., Clough, B., Coates, L. & Wilson, R.J. Enzymes for heme biosynthesis are found in both
746 the mitochondrion and plastid of the malaria parasite *Plasmodium falciparum*. *Protist* **155**, 117-
747 125 (2004).
748 65. Sheiner, L., Vaidya, A.B. & McFadden, G.I. The metabolic roles of the endosymbiotic organelles
749 of Toxoplasma and *Plasmodium*spp. *Current Opinion in Microbiology* **16**, 452-458 (2013).
750 66. Wu, H., Carvalho, P. & Voeltz, G.K. Here, there, and everywhere: The importance of ER
751 membrane contact sites. *Science* **361**, eaan5835 (2018).
752 67. Lee, S. & Min, K.T. The Interface Between ER and Mitochondria: Molecular Compositions and
753 Functions. *Mol Cells* **41**, 1000-1007 (2018).
754 68. Burgoyne, T., Patel, S. & Eden, E.R. Calcium signaling at ER membrane contact sites. *Biochimica*
755 *et Biophysica Acta (BBA) - Molecular Cell Research* **1853**, 2012-2017 (2015).
756 69. de Brito, O.M. & Scorrano, L. Mitofusin 2 tethers endoplasmic reticulum to mitochondria.
757 *Nature* **456**, 605-610 (2008).
758 70. Voleman, L. & Doležal, P. Mitochondrial dynamics in parasitic protists. *PLoS Pathog* **15**,
759 e1008008 (2019).
760 71. Elbaz-Alon, Y. *et al.* Lam6 Regulates the Extent of Contacts between Organelles. *Cell Reports* **12**,
761 7-14 (2015).
762 72. Santos, H.J. & Nozaki, T. Interorganellar communication and membrane contact sites in
763 protozoan parasites. *Parasitology International* **83**, 102372 (2021).

764 73. Lahiri, S. *et al.* A conserved endoplasmic reticulum membrane protein complex (EMC) facilitates
765 phospholipid transfer from the ER to mitochondria. *PLoS biology* **12**, e1001969 (2014).
766 74. Jumper, J. *et al.* Highly accurate protein structure prediction with AlphaFold. *Nature* **596**, 583-
767 589 (2021).
768 75. Zardecki, C. *et al.* PDB-101: Educational resources supporting molecular explorations through
769 biology and medicine. *Protein Science* **31**, 129-140 (2022).
770 76. Araiso, Y. *et al.* Structure of the mitochondrial import gate reveals distinct preprotein paths.
771 *Nature* **575**, 395-401 (2019).
772 77. Webster, M., Witkin, K.L. & Cohen-Fix, O. Sizing up the nucleus: nuclear shape, size and nuclear-
773 envelope assembly. *J Cell Sci* **122**, 1477-1486 (2009).
774 78. Boltryk, S.D. *et al.* CRISPR/Cas9-engineered inducible gametocyte producer lines as a valuable
775 tool for *Plasmodium falciparum* malaria transmission research. *Nat Commun* **12**, 4806 (2021).
776 79. Gomes, A.R. *et al.* A transcriptional switch controls sex determination in *Plasmodium falciparum*.
777 *Nature* **612**, 528-533 (2022).
778 80. Hollin, T. *et al.* Functional genomics of RAP proteins and their role in mitoribosome regulation in
779 *Plasmodium falciparum*. *Nature Communications* **13**, 1275 (2022).
780 81. Ling, L. *et al.* Genetic ablation of the mitoribosome in the malaria parasite *Plasmodium*
781 *falciparum* sensitizes it to antimalarials that target mitochondrial functions. *Journal of*
782 *Biological Chemistry* **295**, 7235-7248 (2020).
783 82. Ke, H., Dass, S., Morrisey, J.M., Mather, M.W. & Vaidya, A.B. The mitochondrial ribosomal
784 protein L13 is critical for the structural and functional integrity of the mitochondrion in
785 *Plasmodium falciparum*. *Journal of Biological Chemistry* **293**, 8128-8137 (2018).
786 83. Dass, S. *et al.* Transcriptional changes in *Plasmodium falciparum* upon conditional knock down
787 of mitochondrial ribosomal proteins RSM22 and L23. *PLOS ONE* **17**, e0274993 (2022).
788 84. Vaidya, A.B. & Mather, M.W. Mitochondrial Evolution and Functions in Malaria Parasites. *Annual*
789 *Review of Microbiology* **63**, 249-267 (2009).
790 85. Eisenberg-Bord, M. *et al.* Cnm1 mediates nucleus-mitochondria contact site formation in
791 response to phospholipid levels. *J Cell Biol* **220** (2021).
792 86. Desai, R. *et al.* Mitochondria form contact sites with the nucleus to couple prosurvival
793 retrograde response. *Science Advances* **6**, eabc9955.
794 87. Scorrano, L. *et al.* Coming together to define membrane contact sites. *Nat Commun* **10**, 1287
795 (2019).
796 88. Filarsky, M. *et al.* GDV1 induces sexual commitment of malaria parasites by antagonizing HP1-
797 dependent gene silencing. *Science* **359**, 1259-1263 (2018).
798 89. Trager, W. & Jensen, J.B. Human malaria parasites in continuous culture. *Science* **193**, 673-675
799 (1976).
800 90. Ribaut, C. *et al.* Concentration and purification by magnetic separation of the erythrocytic stages
801 of all human *Plasmodium* species. *Malaria journal* **7**, 1-5 (2008).
802 91. Willingham, M.C. & Rutherford, A.V. The use of osmium-thiocarbohydrazide-osmium (OTO) and
803 ferrocyanide-reduced osmium methods to enhance membrane contrast and preservation in
804 cultured cells. *Journal of Histochemistry & Cytochemistry* **32**, 455-460 (1984).
805 92. Reynolds, E.S. The use of lead citrate at high pH as an electron-opaque stain in electron
806 microscopy. *J Cell Biol* **17**, 208-212 (1963).
807 93. Huxley, H.E. & Zubay, G. Preferential Staining of Nucleic Acid-Containing Structures for Electron
808 Microscopy. *The Journal of Biophysical and Biochemical Cytology* **11**, 273-296 (1961).